Cargo competition for a dimerization interface restricts and stabilizes a bacterial protease adaptor

Nathan J. Kuhlmann[a,b], Dylan Doxsey[a], and Peter Chien[a,b,1]

[a]Department of Biochemistry and Molecular Biology, University of Massachusetts Amherst, Amherst, MA 01003; and [b]Molecular and Cellular Biology Program, University of Massachusetts Amherst, Amherst, MA 01003

Edited by Brenda A. Schulman, Max Planck Institute of Biochemistry, Martinsried, Germany, and approved March 16, 2021 (received for review May 24, 2020)

Bacterial protein degradation is a regulated process aided by protease adaptors that alter specificity of energy-dependent proteases. In *Caulobacter crescentus*, cell cycle–dependent protein degradation depends on a hierarchy of adaptors, such as the dimeric RcdA adaptor, which binds multiple cargo and delivers substrates to the ClpXP protease. RcdA itself is degraded in the absence of cargo, and how RcdA recognizes its targets is unknown. Here, we show that RcdA dimerization and cargo binding compete for a common interface. Cargo binding separates RcdA dimers, and a monomeric variant of RcdA fails to be degraded, suggesting that RcdA degradation is a result of self-delivery. Based on HDX-MS studies showing that different cargo rely on different regions of the dimerization interface, we generate RcdA variants that are selective for specific cargo and show cellular defects consistent with changes in selectivity. Finally, we show that masking of cargo binding by dimerization also limits substrate delivery to restrain overly prolific degradation. Using the same interface for dimerization and cargo binding offers an ability to limit excess protease adaptors by self-degradation while providing a capacity for binding a range of substrates.

AAA+ | ClpXP | adaptor protein | cell cycle | proteolysis

Controlled protein degradation regulates key physiological processes in all domains of life. In bacteria, AAA+ (ATPases with Associated Activities) proteases control the regulated destruction of misfolded and native substrates to manage cellular stress responses, cell cycle progression, physiological development, and general protein quality control maintenance (1). The Hsp100/Clp family of proteases, which includes the AAA+ protease ClpXP, share structural features and are critical for degrading factors to promote normal cell physiology in bacteria and organelles (2, 3). These energy-dependent machines recognize substrates using an oligomeric unfoldase, which translocates these targets into peptidase chambers that nonspecifically cleave proteins into smaller fragments (4).

To ensure that only specific proteins are degraded by the protease complex, bacteria make use of additional accessory factors, called adaptors, that tune the substrate specificity of the protease (5). Many adaptors act as scaffolds, tethering specific targets to the protease and increasing local concentration to drive degradation. One such example is the SspB adaptor, which binds and scaffolds ssrA-tagged substrates and the extracytoplasmic stress response factor N-RseA to ClpXP (6–8). In *Caulobacter crescentus*, adaptors can work additively to provide increasing levels of substrate specificity to the ClpXP protease (9). In this system, the CpdR adaptor activates ClpX and promotes binding of the RcdA adaptor (10–12). RcdA can bind a third adaptor, PopA, which requires cyclic-di-guanosine monophosphate to promote degradation of CtrA, a major regulator of the *Caulobacter* cell cycle (10, 13–18). In the absence of PopA, RcdA can also deliver substrates, such as the polar cue dependent chromosome segregation protein SpbR (originally annotated as CC2323) (9, 19) and the stalk synthesis protein TacA (9, 20, 21).

RcdA was crystallized as a homodimer, where two three-helix bundle subunits dimerize via conserved hydrophobic residues in the second helix (22). The disordered C terminus is necessary for interactions with CpdR/ClpX, for delivery of all RcdA-dependent cargo, and for self-degradation (9, 22, 23). Upon cargo binding, the CpdR-mediated degradation of RcdA is suppressed, but how this self-degradation is regulated is unclear (23). Direct binding between RcdA and its cargo has been shown using purified components (9, 23), but the details of how RcdA binds and regulates the turnover of a diverse range of cargo remains uncertain.

Here, we show that cargo binding competes with RcdA dimerization by competition for overlapping interfaces. Based on biophysical measurements, we determine that while RcdA is a dimer in solution on its own, the adaptor binds cargo as a monomer. We generate a constitutively monomeric variant by mutating the predicted dimer interface and show that RcdA dimerization is required for self-degradation. Interestingly, this variant is deficient in delivering the substrates SpbR and TacA for degradation but facilitates PopA-dependent CtrA degradation as normal. We use hydrogen–deuterium exchange mass spectrometry (HDX-MS) to map regions of RcdA important for cargo binding and find that different substrates rely on different sites of the dimer interface. Mutations at these regions result in adaptor variants that are defective for degradation of specific substrates, and expression of these variants alters cell physiology consistent with this change in specificity. Taken together, our data show how RcdA can deliver either cargo or itself for degradation and how a large interface, normally masked by dimerization, can be used to capture a range of substrates.

Results

Cargo Binding Competes with RcdA Dimerization. Previous studies have established RcdA as a homodimeric protein in solution (22) that can directly bind to its cargo (9). We began our studies by

Significance

Energy-dependent proteases broadly regulate bacterial physiology and development. Adaptor proteins tune the substrate specificity of proteases by selectively delivering cargo and themselves can be degraded. We find that the RcdA adaptor forms homodimers that are degraded by the ClpXP protease. Cargo binding disrupts the dimer interface, stabilizing the adaptor, and provides a model for how adaptor degradation can be controlled. Mapping the surfaces responsible for cargo binding shows that different overlapping regions of the dimer interface are tailored to different substrates. Our results suggest a mode of control that provides robust adaptor activity subject to buffering by cargo demand.

Author contributions: N.J.K. and P.C. designed research; N.J.K. and D.D. performed research; N.J.K. contributed new reagents/analytic tools; N.J.K., D.D., and P.C. analyzed data; and N.J.K. and P.C. wrote the paper.

The authors declare no competing interest.

This article is a PNAS Direct Submission.

[1]To whom correspondence may be addressed. Email: pchien@umass.edu.

This article contains supporting information online at https://www.pnas.org/lookup/suppl/doi:10.1073/pnas.2010523118/-/DCSupplemental.

Published April 19, 2021.

exploring RcdA–cargo binding using size-exclusion chromatography coupled with multiangle light scattering (SEC-MALS) to measure absolute molar mass. SpbR, a RcdA-dependent cargo responsible for inhibiting centromere translocation (19), is a 42 kDa monomer in solution, while, as expected, the molar mass of RcdA is a dimer (36 kDa, Fig. 1*A*). The combination of both proteins results in a complex with a determined mass of 61 kDa (Fig. 1*A*). Our data is consistent with a monomer of RcdA (17 kDa) binding a monomer of SpbR (44 kDa) and inconsistent with a dimer of RcdA binding a monomer of SpbR (a predicted mass of 77 kDa) (Table 1). We confirmed this monomer:monomer stoichiometry by using analytical ultracentrifugation and found a similar mass of 60 kDa for the RcdA:SpbR complex (Fig. 1*D*).

We next tested other RcdA cargo. PopA, the RcdA-binding adaptor, shows an experimental mass of 41 kDa (Fig. 1*A*). In the presence of RcdA, the complex mass is 58 kDa, consistent with a monomer of PopA (41 kDa) binding a monomer of RcdA (17 kDa) (Fig. 1*A* and Table 1). TacA, a transcription factor involved in stalk biogenesis, has an experimental molar mass consistent with a dimer (124 kDa). When bound to RcdA, the complex shows an apparent mass of 141 kDa, again consistent with a monomer of RcdA binding to a dimer of TacA (Fig. 1*A* and Table 1). Strangely, despite having more mass than RcdA, we noticed that both PopA and SpbR elute after RcdA on our SEC columns, which we attribute to nonspecific interactions with the stationary phase of our column or to PopA and SpbR having different physical shapes than the RcdA dimer. We confirmed the presence of both cargo and adaptor in these complexes by sodium dodecyl sulphate-polyacrylamide gel electrophoresis (*SI Appendix* and Fig. 2).

Using isothermal calorimetry, we determined that the dimerization constant of RcdA (K_D = 7 μM, Fig. 1*B*) and dissociation constant between RcdA and SpbR (K_D = 1 μM, Fig. 1*C*) were of similar order. Measurements with a labeled RcdA reporter using fluorescence polarization also revealed similar magnitudes for dimerization (K_D = 2.5 μM) and SpbR binding (K_D = 2.1 μM) (Fig. 1*E*). Finally, microscale thermophoresis measurements provide additional confirmation that RcdA binds itself and SpbR with similar ranges of affinity (RcdA–SpbR complex [average K_D = 5 μM]; dimerization [average K_D = 3 μM]) (*SI Appendix*, Fig. S1).

Taken together, these data suggest that RcdA binds cargo as a monomer and that binding of cargo competes with dimerization with similar binding affinities (Fig. 1*F*).

RcdA Dimerization Is Necessary for Its Own Degradation. Previous studies have shown RcdA is itself degraded by the CpdR-activated ClpXP protease (Fig. 2*A*) but that cargo binding inhibits self-degradation (Fig. 2*B*) (23). Interestingly, this stabilization occurs even for nondegradable substrates (Fig. 2*B* and *SI Appendix*, Fig. S3*A*) (23), which we did not have a mechanistic explanation for at the time. Because our findings reveal that cargo binding to RcdA causes adaptor monomerization, we hypothesize that RcdA dimers are degraded because one subunit of RcdA delivers the other and cargo binding results in displacing the normally delivered protomer (Fig. 2*A*). Consistent with this reasoning, a version of RcdA that lacks the C-terminal motif needed for tethering, but still capable of dimerization (22, 23), is not degraded in the presence of full-length RcdA and appears to suppress degradation of the native protein (*SI Appendix*, Fig. S3), suggesting that only full-length RcdA homodimers are competent for degradation.

To more completely test this hypothesis, we generated a monomeric RcdA variant by mutating a leucine in the dimer interface (as determined from the reported crystal structure [Protein Data Bank: 3CTW (22)] to a glutamic acid (Fig. 2*C*). In contrast to the wild-type dimer mass (35 kDa), RcdA-L82E behaved as a 19 kDa monomer (Fig. 2*C*) and failed to form dimers with itself or with wild-type RcdA by fluorescence polarization (*SI Appendix*, Fig. S3*E*). The monomeric L82E variant was also completely stable in vitro in the presence of ClpXP and CpdR (Fig. 2*B*). Finally, while wild-type RcdA is degraded in vivo, RcdA L82E is not (*SI Appendix*, Fig. S3*G*). These data support a model where dimerization of RcdA is necessary for its self-delivery to the ClpXP protease for degradation.

The L82E Variant Is Defective in Some Cargo Binding and Delivery. We next tested the ability of RcdA L82E to bind and deliver different RcdA cargo. SpbR and TacA are substrates of ClpXP that require RcdA for efficient degradation, while PopA is an adaptor that binds RcdA to expand its substrate profile (9). We used wild-type RcdA or RcdA L82E labeled with fluorescein and fluorescence polarization as a proxy for cargo binding. Using this assay, we found that wild-type RcdA bound all three cargo (^{DBD}TacA is the minimal domain of TacA needed for RcdA degradation, where DBD is the DNA-binding domain of TacA) (Fig. 3*A* and *SI Appendix*, Fig. S4*B*). The monomeric RcdA L82E was unable to form a complex with SpbR and ^{DBD}TacA but, surprisingly, bound PopA with affinity equivalent to wild-type RcdA (Fig. 3*A* and *SI Appendix*, Fig. S4*B*). SEC-MALS and sodium dodecyl sulphate-polyacrylamide gel electrophoresis analysis of fractions confirmed these changes in cargo binding (Fig. 3*B* and *SI Appendix*, Fig. S4 *A* and *F*).

Consistent with the defects in SpbR and TacA binding, the RcdA L82E variant showed less stimulation of the CpdR-ClpXP–mediated degradation of these substrates in vitro (Fig. 3*C* and *SI Appendix*, Fig. S4*G*). This deficiency was not due to a failure of RcdA L82E to bind the CpdR-ClpX complex, as fluorescence polarization assays that monitor ClpX:CpdR:RcdA ternary complex formation (9) showed that both RcdA variants were able to bind the ClpX:CpdR complex with similar affinity (*SI Appendix*, Fig. S5).

PopA binds RcdA directly and, in a c-di-guanosine monophosphate dependent manner, promotes degradation of CtrA (16, 17). To test the effects on PopA-mediated substrate delivery, we used a GFP (green fluorescent protein) reporter fused to the minimal domains of CtrA needed for regulated degradation (GFP-CtrARD+15) (18). Unlike the case for TacA or SpbR, the RcdA L82E variant was capable of stimulating PopA-mediated CtrA degradation (Fig. 3*D* and *SI Appendix*, Fig. S4*E*). These data show that disrupting the dimer interface of RcdA reduces binding to some substrates, but this monomeric variant can still bind to an activated ClpXP and deliver permissive substrates (such as CtrA). Consistent with an overlap in interfaces for cargo and dimerization, locking RcdA into a dimer by cross-linking also prevents cargo binding, while L82E treated with the same concentrations of glutaraldehyde did not affect the L82E variant's ability to bind PopA (Fig. 3*E* and *SI Appendix*, Fig. S5*D*). Taken together with the observation that all cargoes can compete with RcdA dimerization (Fig. 1), our emerging model is that different substrates rely on different regions of the RcdA dimer interface.

The Dimer Interface Is Protected from Exchange in the Presence of Cargo. To determine how different cargoes interact with RcdA, we used HDX-MS, which measures differences in deuterium uptake in the peptide backbone to determine protein–protein interaction surfaces (24, 25). We first compared high and low concentrations of RcdA to map the dimer interface (*SI Appendix*, Fig. S6*A*) and found these data to be consistent with the comparison between monomeric RcdA L82E and the dimeric wild-type RcdA that also highlights the dimerization interface (Fig. 4*A*). We then measured deuterium uptake of RcdA incubated with excess ^{DBD}TacA or PopA to define potential interaction surfaces with these cargoes (Fig. 4*A*). Each condition is summarized in a differential deuterium uptake plot as a heatmap showing percent deuterium uptake for each peptide and regions of largest protection (>15%) mapped onto a surface rendition of a RcdA monomer (Fig. 4*A*). Individual deuterium uptake plots for selected regions of largest protection are provided in Fig. 4*B* and *SI Appendix*, Fig. S6*C*.

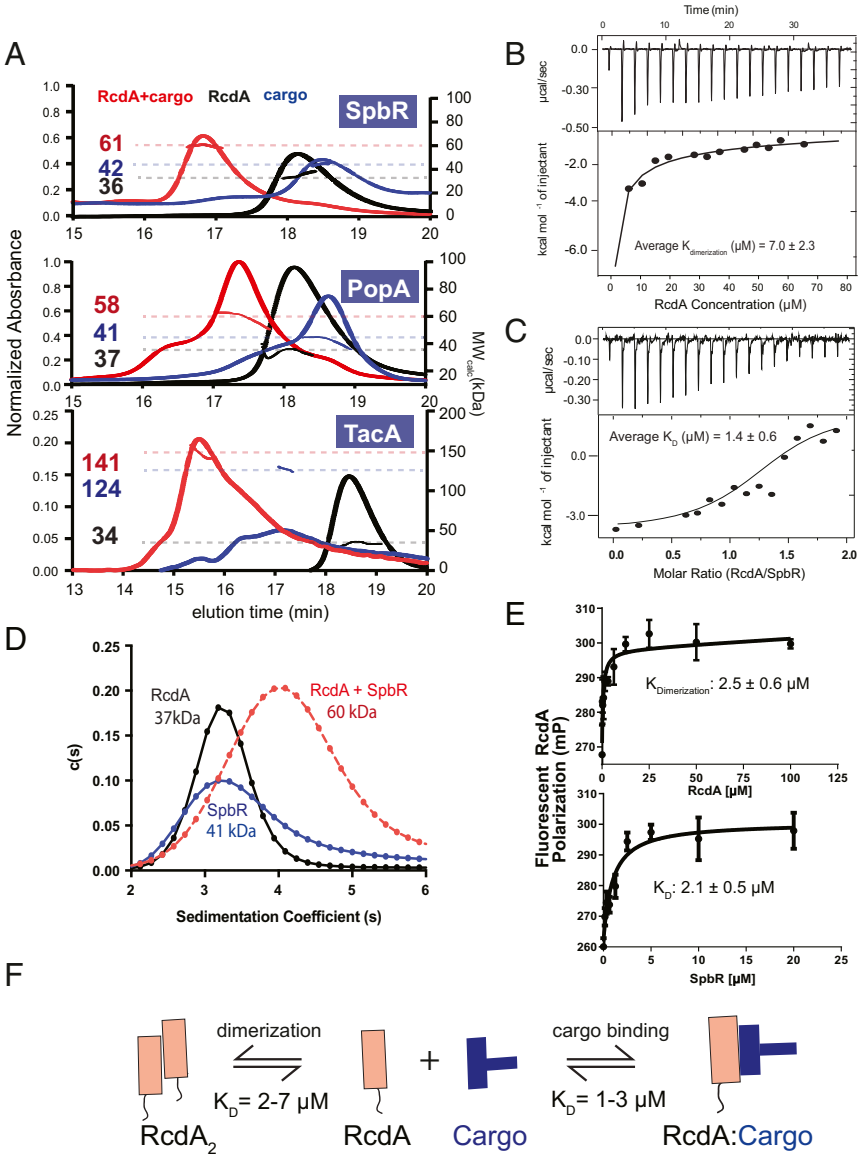

Fig. 1. Cargo binding competes with RcdA dimerization. (*A*) SEC-MALS traces of different RcdA–cargo complexes. Representative SEC-MALS traces of the RcdA, cargo, and the RcdA–cargo complexes. Left axes show normalized absorbance traces, and right axes show calculated molecular weight in kilodaltons. Dashed lines connect the scattering traces of the proteins/complexes with the calculated molecular weights as labeled. The colored lines under each peak represent the collected light scattering data as a distribution of molecular weights over the width of the chromatography peak. Numbers represent the calculated molecular weight from the scattering data. Concentrations of each component and complex are noted in the *Methods* section. (*B*) Representative ITC thermogram of the heat of RcdA dissociation; heats of injection are shown on the top. The sample syringe was loaded with 400 µM RcdA and titrated into a cell containing buffer. $K_{Dimerization}$ values are the average of three independent replicates with error representing SD. (*C*) Representative ITC thermogram of the SpbR-RcdA complex formation; heats of injection are shown on the top. The sample syringe was loaded with 400 µM RcdA and titrated into a cell containing 40 µM SpbR. K_D values are the average of three independent replicates with error representing SD. ITC data shown are derived from a single titration with average RcdA heat of dimerization subtracted (*SI Appendix*, Fig. S1 for all titrations). (*D*) Sedimentation constants fitted from velocity ultracentrifugation of the RcdA–SpbR complex. Each component was present at 25 µM, either alone or in complex. (*E*) Fluorescence polarization of 100 nM fluorescein-labeled RcdA at different concentrations of either RcdA (*Top*) or SpbR (*Bottom*), with the average and SD of triplicate experiments. $K_{Dimerization}$ for RcdA dimerization and K_D for RcdA:SpbR binding were derived as described in *Methods*. (*F*) Cartoon illustrating the competition between dimerization and cargo binding. All RcdA concentrations are in terms of monomeric equivalents unless otherwise noted.

Based on the Protein Data Bank ePISA server and the 3CTW crystal structure of RcdA, the most buried residues in the dimer interface lie between residues 34 to 45 and 71 to 101 (*SI Appendix*, Fig. S6*B*). We validated this in solution with our HDX-MS data, which highlights residues 26 to 44 and 80 to 97 as being most protected in the wild-type dimer (Fig. 4*A*). This result further confirms how the L82E mutation disrupts the dimer interface to generate a monomeric variant. Consistent with our biochemical results in Fig. 3, ^{DBD}TacA also binds the region of the dimer interface containing the L82 residue with most protection at residues 79 to 101, supporting our observation that RcdA L82E fails to deliver TacA for degradation. Interestingly, PopA also binds the dimer interface but principally protects residues 26 to 70, with the L82-containing region of RcdA showing no substantial protection. We conclude that, consistent with our biochemical data, TacA and PopA both bind the RcdA homodimer interface to disrupt dimerization, but they bind at different regions of this interface.

Table 1. Cargo binding competes with RcdA dimerization

	Experimental (kDa) (±4 kDa)	Stoichiometry	Predicted (kDa)
RcdA	36	RcdA2 (dimer)	37
		RcdA (monomer)	19
SpbR	42	SpbR (monomer)	43
RcdA + SpbR	61	RcdA:SpbR	62
TacA	124	TacA2 (dimer)	127
RcdA + TacA	141	RcdA:TacA2	146
PopA	41	PopA (monomer)	47
RcdA + PopA	58	RcdA:PopA	66

Table of molecular weights of the different RcdA–cargo complexes. The experimental column shows the complex mass measured by SEC-MALS. The stoichiometry column gives the stoichiometry of each protein consistent with the experimental mass. The predicted column lists the Expert Protein Analysis System (EXPASY) predicted mass of each stoichiometry listed. Bolded text is the experimentally measured complex masses displayed in Fig. 1.

Mutations in the PopA Interaction Region Highlight Differences in Cargo Binding. Our HDX-MS data highlights two regions in RcdA as protected upon PopA binding, one of which includes a cluster of highly conserved basic residues (R49, K53, and R57) (*SI Appendix*, Fig. S7*A*). We mutated these residues to glutamic acid to generate a variant that we refer to as RcdA 3E for brevity (Fig. 5*A*). Based on our biochemical studies (Fig. 3), we predict that both TacA and SpbR bind similar regions of RcdA, including L82, that are distinct from the regions preferred by PopA (Fig. 4). Consistent with this hypothesis, while the RcdA 3E fails to bind PopA based on SEC-MALS, it forms a complex and coelutes with SpbR with a measured mass consistent with the native complex and a dimer of

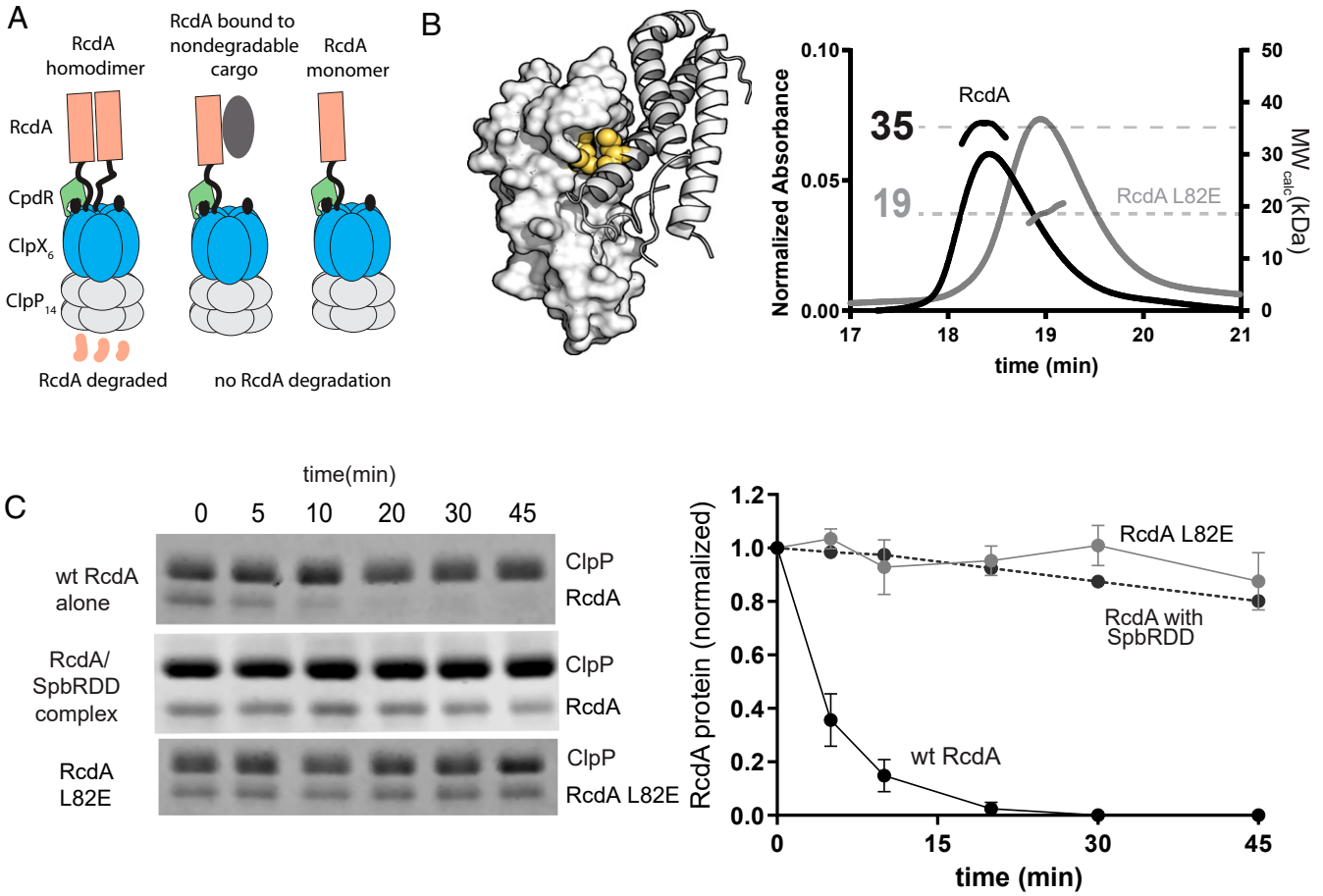

Fig. 2. Dimerization is necessary for RcdA degradation. (*A*) Illustration of the proposed degradation model of RcdA dimers, RcdA bound to cargo, or RcdA monomers. (*B*) SEC-MALS trace of 25 μM RcdA and 25 μM RcdA L82E. The shaded lines under each peak represent the collected light scattering data as a distribution of molecular weights over the width of the chromatography peak. Numbers represent the calculated molecular weight from the scattering data. Illustration of the L82 residue (in yellow) in the RcdA (Protein Data Bank ID: 3CTW) crystal structure where one monomer is surface rendered and the other is in cartoon. (*C*) In vitro gel-based degradation of 3 μM RcdA alone, 3 μM RcdA with 3 μM SpbRDD, or 3 μM RcdA L82E alone. Quantification of three independent replicates is shown on the right; error bars represent SD. Coomassie-stained gels were visualized using an Odyssey imaging system for better detection of the RcdA band. *SI Appendix*, Fig. S3 for full gels.

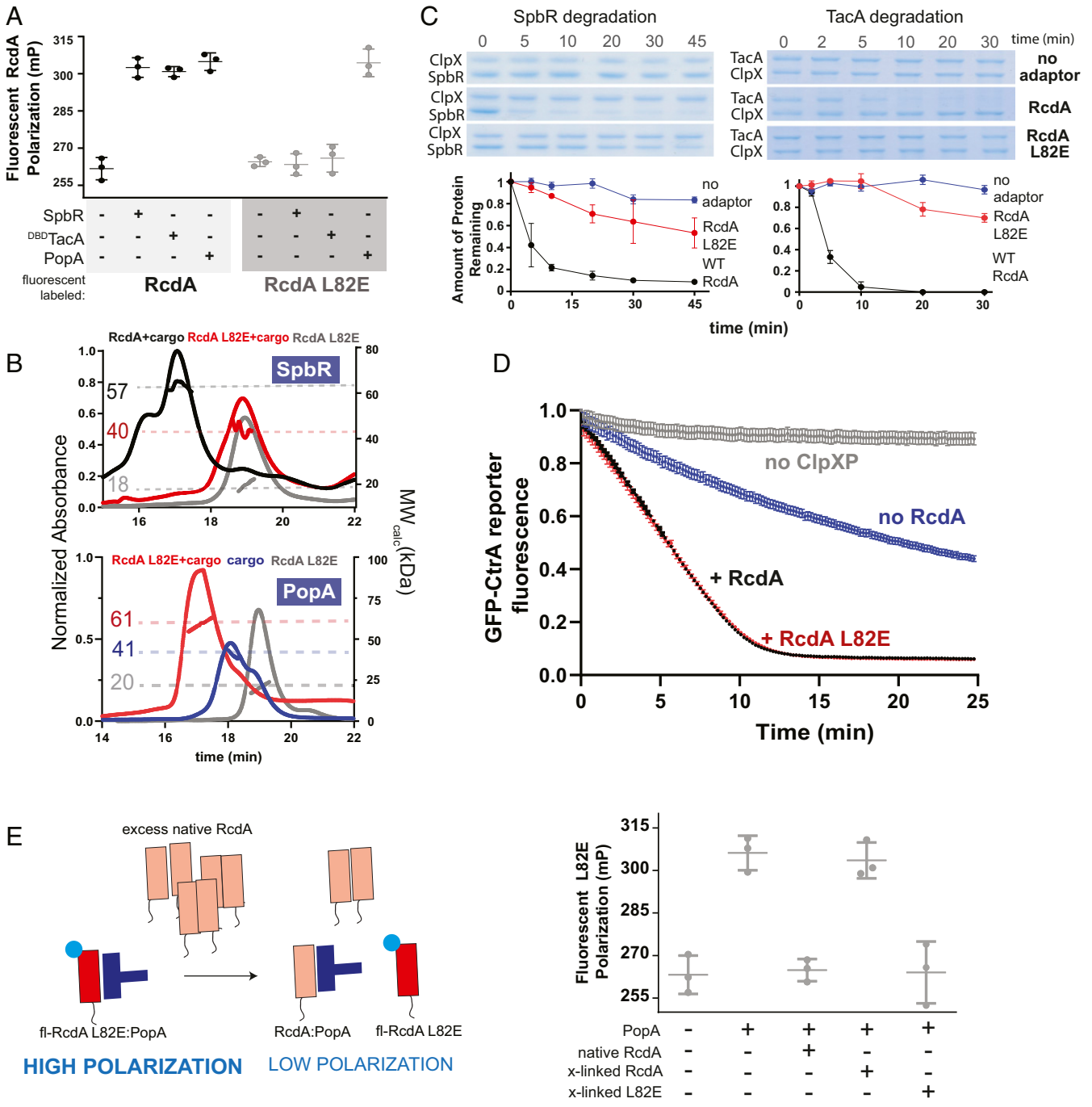

Fig. 3. The L82E variant shows differences in cargo binding and RcdA activity. (*A*) Fluorescence polarization of labeled RcdA (black) or RcdA L82E (gray) in the presence of SpbR, ^{DBD}TacA, and PopA; 100 nM of each labeled reporter was incubated with 20 μM cargo for 45 min, and the polarization of labeled RcdA or RcdA L82E was measured. Three independent replicates are shown with average and SD. (*B*) Representative SEC-MALS chromatograms of RcdA L82E in the presence of SpbR or PopA. Wild-type RcdA incubated with SpbR, PopA alone, and RcdA L82E alone are shown for comparison. The colored lines under each peak represent the collected light scattering data as a distribution of molecular weights over the width of the chromatography peak. Numbers represent the calculated molecular weight from the scattering data. (*C*) In vitro gel-based degradation assay of SpbR or in the presence of RcdA or RcdA L82E. Full gels are shown in *SI Appendix*, Fig. S3. Quantification of three independent replicates showing means and error bars (SD). (*D*) In vitro fluorescence degradation assay of GFP-CtrARD+15 in the presence of RcdA or RcdA L82E. Each fluorescence trace is the average of three independent replicates with error bars showing SD. (*E*, *Left*) Illustration of assay to determine binding of RcdA to PopA using a fluorescently labeled RcdA L82E. PopA binding to fluorescently labeled RcdA L82E results in high polarization of the RcdA L82E reporter. Native RcdA will bind PopA, resulting in free-labeled RcdA L82E, which has a low polarization signal. (*E*, *Right*) Polarization signal from labeled RcdA L82E in the presence of the indicated components. Note that wild-type RcdA causes a decrease in polarization, while cross-linked RcdA does not, showing that locked RcdA dimers cannot bind cargo. Cross-linked RcdA was generated with 1% gluteraldehyde treatment; see *SI Appendix*, Fig. S5 for more information.

mass consistent with wild-type RcdA (Fig. 5*B* and *SI Appendix*, Fig. S7 *E*, *G*, and *H*). Given the failure to bind PopA, we were not surprised to find that RcdA 3E was unable to deliver CtrA for degradation (Fig. 5*C*). Consistent with the preserved binding to SpbR and TacA, RcdA 3E was active for their degradation, although not to fully wild-type activity (Fig. 5*D*), which we suggest

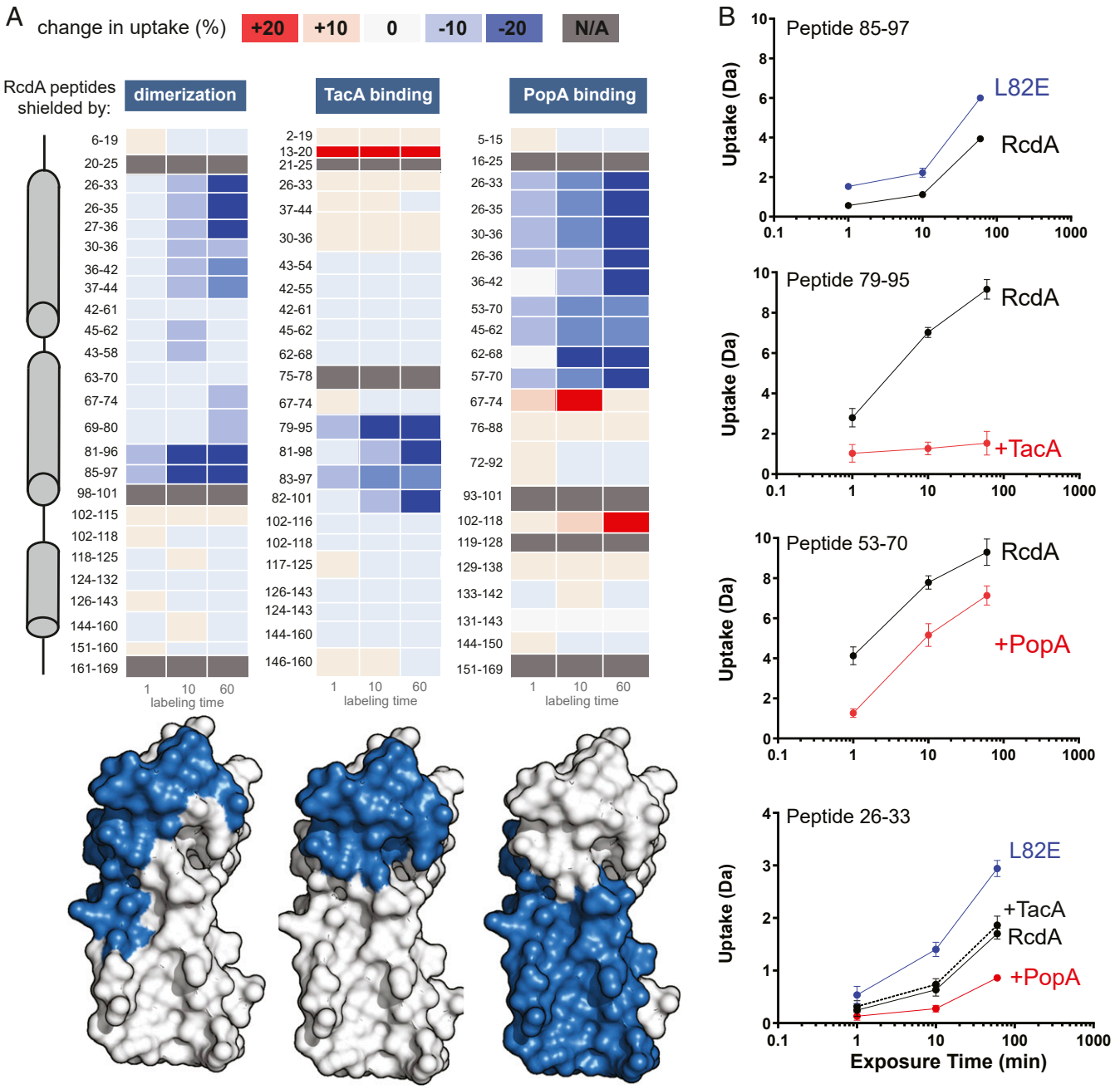

Fig. 4. The dimerization interface is protected from deuterium exchange in the presence of cargo. (*A*) Differential uptake heatmap plots of 15 μM RcdA compared with 15 μM RcdA L82E (dimerization), 600 nM RcdA incubated with 20 μM ^{DBD}TacA (TacA), or 600 nM RcdA incubated with 20 μM PopA (PopA). Regions of 15% or greater protection are highlighted in blue on a surface rendition of the RcdA monomer structure (Protein Data Bank ID: 3CTW). (*B*) Deuterium uptake plots of selected peptides. Data are plotted as the mean of three replicates with the SD plotted as error bars. See *SI Appendix*, Fig. S6 for additional peptides.

may be due to folding defects of the purified protein. Overall, these data suggest that while the homodimer interface of RcdA is generally responsible for cargo binding, PopA and SpbR/TacA rely on different aspects of this interface for effective binding.

Defects in Cargo Binding Affect Target Degradation In Vivo. We finally investigated the in vivo consequences of altering RcdA–cargo interactions. During the cell cycle of *Caulobacter crescentus*, the transition from Gap 1 (G1) to Synthesis phase (S) is accompanied by a morphological change from a motile swarmer cell to a sessile stalked cell, facilitated by degradation of RcdA-dependent substrates. Because of this transition, defects in the cell cycle are often accompanied by changes in morphological features. We generated strains that express RcdA, RcdA L82E, or RcdA 3E at the *xylX* locus in Δ*rcdA* strains, which allows for titration of RcdA using the inducer xylose. Δ*rcdA* strains have longer stalks and reduced growth in low-percentage agar, indicative of defects in cell cycle stages and development of stalk growth (9, 12). At low levels of inducer, RcdA variant levels driven by the *xylX* promoter were similar to that of the wild-type control (*SI Appendix*, Fig. S8*C*), and in these conditions, stalk length was compromised in both RcdA L82E and 3E backgrounds (Fig. 6*A*), while growth in low-percentage agar was more affected in the RcdA 3E mutant (*SI Appendix*, Fig. S8 *A* and *B*). Curiously, under high induction,

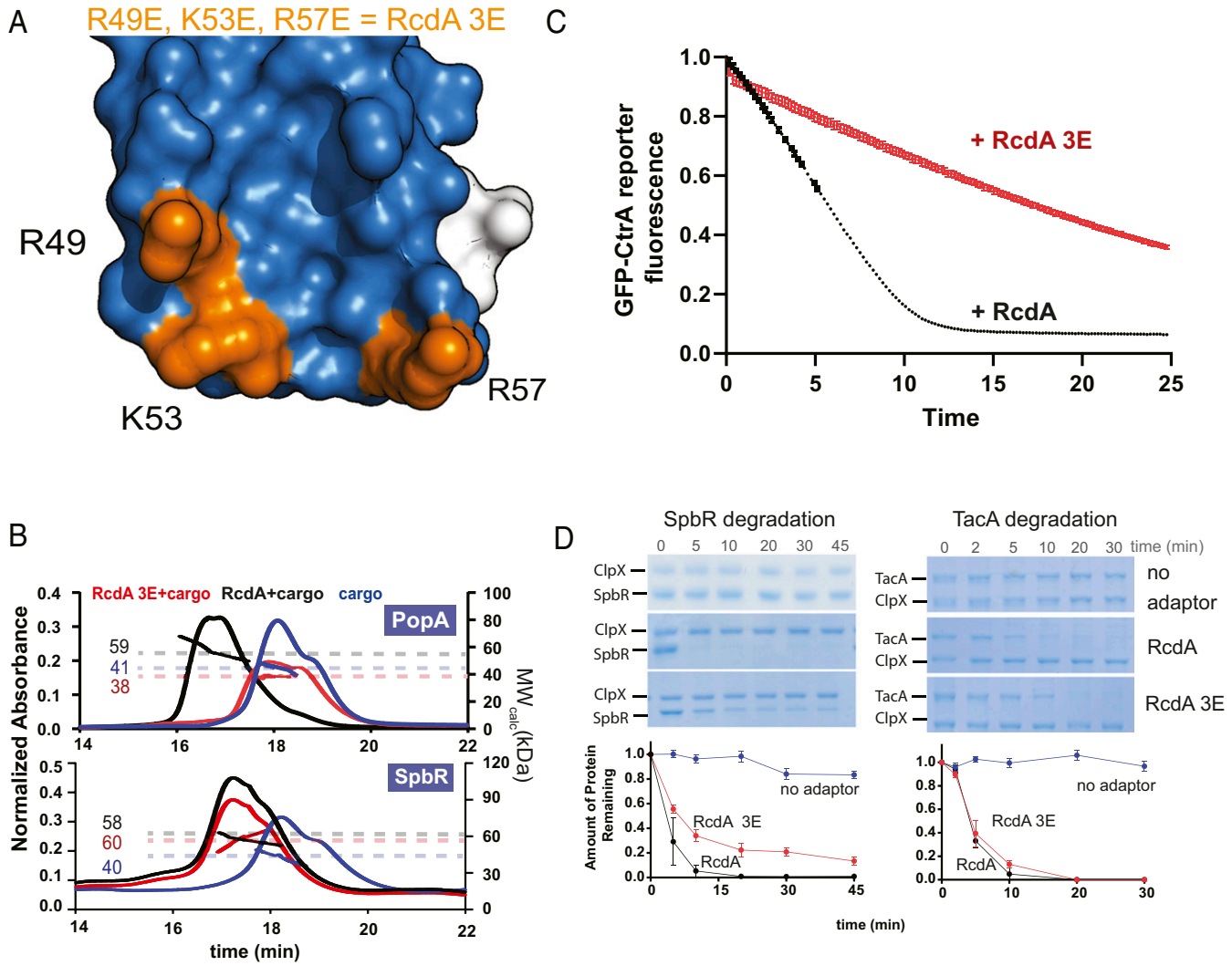

Fig. 5. Mutations in the extended surface highlight differences in cargo selectivity and RcdA activity. (*A*) Illustration of region of RcdA protected upon PopA incubation (in blue). In orange are the three residues (R49, K53, and R57) mutated to glutamic acids in RcdA 3E. (*B*) Representative SEC-MALS traces for the PopA or SpbR mixtures with RcdA 3E (red). The complex of native RcdA and cargo (black) and the cargo alone (blue) is shown for comparison. The colored regions under each peak represent the collected light scattering data as a distribution of molecular weights over the width of the chromatography peak. Numbers represent the calculated molecular weight from the scattering data. (*C*) In vitro fluorescence degradation assay of GFP-CtrARD+15 in the presence of RcdA or RcdA 3E. Fluorescence traces are the average of three independent replicates with error bars showing SD. The +RcdA control is the same control that was used in Fig. 3C and is shown here for comparison to RcdA 3E. (*D*) In vitro gel-based degradation assay of SpbR or TacA in the presence of RcdA or RcdA 3E. Quantification of three independent replicates is shown below. See *SI Appendix*, Fig. S7 for full gels.

where RcdA levels are well above normal, stalk length was reduced to less than wild type for all the alleles tested (including wild-type RcdA) (Fig. 6*A*).

These data suggest that the different substrates stabilized by the different RcdA variants may drive defects in stalk length and agar growth separately. Consistent with this and our in vitro results, in vivo degradation assays showed that strains expressing RcdA L82E are deficient in SpbR degradation (Fig. 6*B*), while strains expressing RcdA 3E failed to degrade CtrA during either asynchronous growth (Fig. 6*B*) or during cell cycle progression (*SI Appendix*, Fig. S8*F*).

Dimerization Limits Overly Prolific RcdA Activity. When we monitored cell cycle progression, we noticed that CtrA levels were slightly lower with RcdA L82E upon minimal induction of this mutant (*SI Appendix*, Fig. S8*F*). Interestingly, in our biochemical studies, we noticed that at lower RcdA concentrations (300 nM), the rate of PopA-mediated CtrA degradation in the presence of RcdA L82E was faster than that found with wild-type RcdA (Fig. 6*C*). When we generated enzyme substrate reaction curves under these conditions and fit to Michaelis–Menten kinetics, we found that RcdA L82E was twofold more active for PopA-mediated CtrA degradation at limiting concentrations of protease and adaptor (Fig. 6*D*). Since the RcdA dimer interface is also used to bind cargo (such as PopA), this observation is most consistent with a model where dimerization normally limits the specific activity of RcdA for cargo delivery.

We further explored this dimerization-driven limit on RcdA activity in normal physiology by constructing merodiploid strains that expressed either wild-type RcdA or RcdA L82E from the native *rcdA* promoter. We found that steady-state levels of CtrA are lower and degraded faster in the RcdA L82E strain than in the wild-type strain (Fig. 6*E*). During synchronized growth, CtrA is lost more rapidly during the G1 to S transition, and reaccumulation of CtrA in

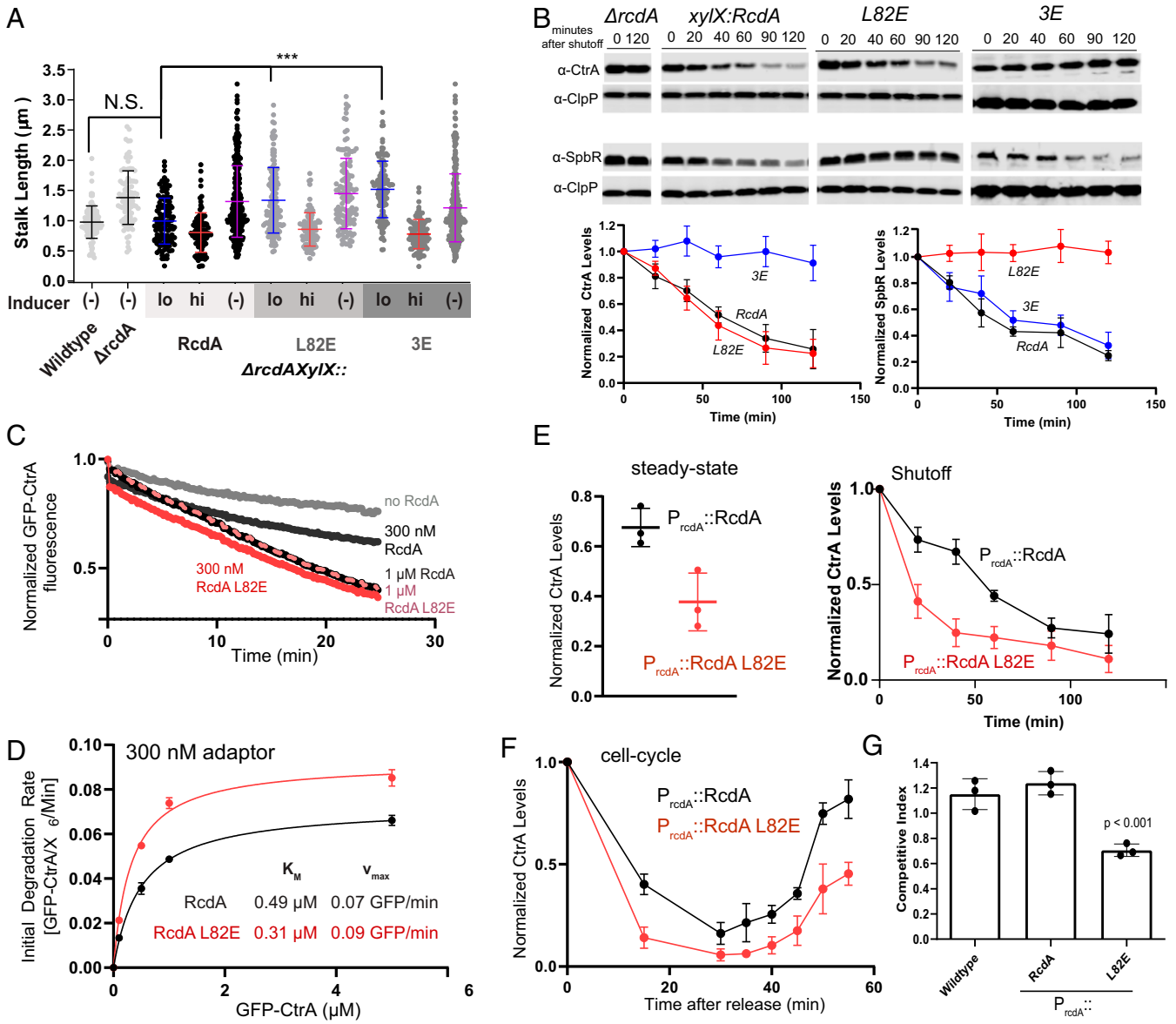

Fig. 6. Disruption of the extended RcdA interaction surface affects normal cell physiology. (*A*) Stalk length quantification and images of cells expressing RcdA, RcdA L82E, or RcdA 3E from the xylose locus. Cells grown to exponential phase in media containing 0.2% (hi: high inducer), 0.002% xylose (lo: low inducer), or 0.2% glucose (repressed). A one-tailed, unpaired *t* test with $\alpha = 0.05$ was used to compare stalk lengths from indicated strains. N.S., not significant. ***$P < 0.001$. (*B*) Chloramphenicol shutoff assays monitoring the degradation of SpbR and CtrA in cells expressing wild-type RcdA or RcdA L82E. (*C*) Normalized fluorescence degradation curves of GFP-CtrA in the presence of different concentrations of RcdA and RcdA L82E. In this experiment, 500 nM PopA, 1 μM cyclic di-guanosine monophosphate, 300 nM RcdA or L82E, 0.1 μM ClpX, 0.2 μM ClpP, and 1 μM GFP-CtrA were used. (*D*) Initial rates of GFP-CtrA degradation as a function of adaptor; 500 nM PopA, 1 μM CdG, 300 nM RcdA or L82E, 0.1 μM ClpX, 0.2 μM ClpP, and varying concentrations of GFP-CtrA reporter were used in these experiments ($n = 3$). Fits are to the Michaelis–Menten equation. (*E*) Normalized CtrA steady levels in asynchronous cultures and their degradation during shutoff (*SI Appendix*, Fig. S7 for full gels) or (*F*) during cell cycle progression in a P_{rcdA}::RcdA or P_{rcdA}::RcdA L82E strain background. (*G*) Fitness competition assay between wild type and P_{rcdA}::RcdA or P_{rcdA}::RcdA L82E. For all data except the asynchronous shutoff, which were duplicate experiments, average and SD of three independent replicates are shown.

predivisional cells is reduced (Fig. 6*F* and *SI Appendix*, Fig. S8*G*). Finally, to determine the overall fitness cost of this mutation, we used a competition assay and found that strains expressing only RcdA L82E are at a fitness disadvantage compared to wild type (Fig. 6*G*). Taken together with our biochemical results, these data suggest that dimerization limits RcdA activity, and bypassing this restriction results in persistent degradation of substrates such as CtrA.

Discussion

Adaptor-mediated degradation is critical for bacteria. Our results demonstrate a surprising feature of the cell cycle adaptor system in *Caulobacter*, where binding of a cargo to the RcdA adaptor competes with homodimerization. This competition results in stabilization of RcdA, protecting it from self-degradation by ClpXP while providing a relatively broad binding surface for cargo binding. We note that the cellular concentration of RcdA estimated by ribosome profiling is 6 μM, and estimated concentrations of SpbR, PopA, and TacA are between 2 and 4 μM each (26). This implies that total cargo concentration is likely in excess of RcdA, driving the RcdA equilibrium toward the monomer form and protecting RcdA from degradation until target substrates are delivered by RcdA. Our binding data are consistent with the

model that different classes of cargo can interact with specific regions of this surface, with our direct measurement by HDX-MS and our mutation data showing that we can selectively influence particular substrate binding and degradation (Fig. 7). Interestingly, CpdR and RcdA are conserved throughout α-proteobacteria, while PopA is only present in *Caulobacter* and closely related bacteria (16, 27). The region mutated in our RcdA 3E variant may represent the binding interface for currently unknown adaptors that fulfill the role for PopA in other species where CtrA is degraded, such as Sinorhizobium meliloti (28). Recent structures show that the E3 ubiquitin ligase adaptor Skp1 buries its F-box interaction site upon dimerization (29), illustrating that masking of cargo binding sites by self-interactions can be generally found in biological systems.

Because protease adaptors catalyze the irreversible destruction of targets, we also considered how dimerization of RcdA could regulate adaptor activity. Our results support two mechanisms for the role of dimerization in restricting adaptor activity.

First, because the RcdA homodimer is degraded robustly, overlapping the dimer interface and cargo binding site adjusts RcdA levels tuned to substrate availability. Our results show that RcdA monomers are not degraded and that binding to cargo results in loss of RcdA dimerization. Once the substrates are degraded, RcdA homodimers would form more readily and be destroyed. Similarly, RcdA would never be fully eliminated as, once levels drop below the dimerization constant, the shift to the monomeric species would stabilize the adaptor.

Second, masking substrate interaction surfaces by dimerization appears to limit degradation of substrates directly, as seen with accelerated PopA-mediated CtrA proteolysis in the presence of the monomeric RcdA variant (Fig. 6). Essentially, the partner monomer of a homodimer acts as an inhibitor of cargo binding, resulting in reduced degradation of substrates. Our data show that there are physiological consequences to the loss of this limitation, as cells expressing only monomeric RcdA have lower levels and faster degradation of the essential transcription factor, CtrA, resulting in reduced fitness. We note that other protease systems show similar constraints; for example, the N-domain of the Lon protease interacts both with itself and some substrates (30).

Not all dimeric adaptors share this competitive mechanism. For example, the SspB adaptor delivers proteins marked by the ssrA-tagging system to the ClpXP protease (6, 31–33). Unlike RcdA, SspB binds substrates at sites far away from the dimer interface (7), and SspB delivery is optimal when two molecules of substrates are bound per SspB dimer (32, 33). Therefore, SspB activity would not be limited by competition from dimer formation. We reason that because ssrA-tagged proteins naturally arise from failed translation (34, 35), these targets should always be destroyed; therefore, prolific SspB activity would not be toxic. By contrast, degradation of RcdA-dependent substrates occurs only at a specific stage of the cell cycle (9, 12), and additional controls to limit this adaptor activity, such as the mechanism we describe here, would be beneficial. We speculate that other adaptors that deliver substrates in such a highly timed manner may also be subject to similar regulation.

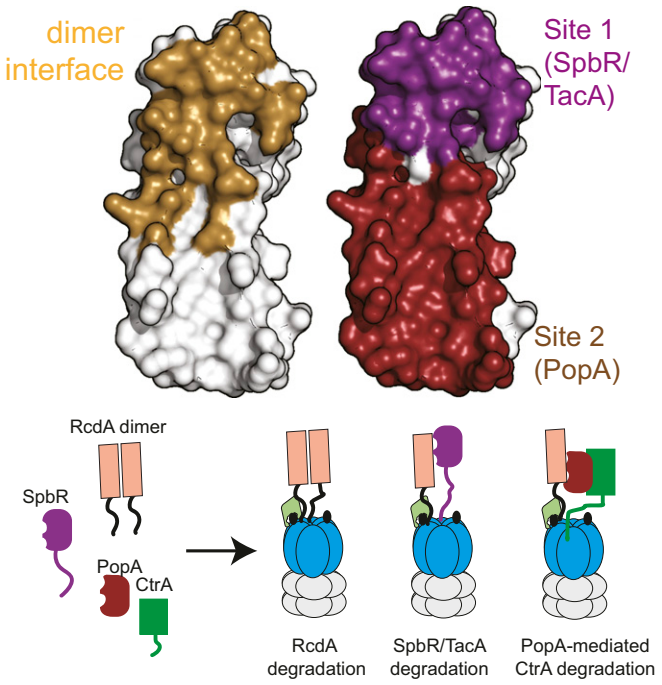

Fig. 7. Model of RcdA binding and delivery mechanism. The highlighted structure illustrates the different interaction sites of RcdA. In gold is the dimer interface. In purple is the site involved in the SpbR and TacA interaction, which includes the L82 residue. In ruby is the site involved in the PopA interaction, which includes residues R49, K53, and R57. The cartoon model shows how the oligomerization state of RcdA affects its activity and self-degradation. When not bound to cargo, RcdA is dimeric and delivered to a CpdR-bound ClpXP for degradation. Cargo binding at different interaction sites by different cargo (SpbR/TacA or PopA) causes dissociation of the RcdA dimer and masks RcdA from its own degradation.

Methods

Protein Expression and Purification. BL21(DE3) *pLYS* or X90 cells with expression plasmids for different proteins were grown at 37 °C to an optical density$_{600}$ of 0.4 to 0.6 and then induced with 0.4 mM isopropyl thiogalactopyranoside (IPTG) for 3 to 4 h. Induced cells were then centrifuged at 7,000 × *g* for 10 min, resuspended in buffer containing 50 mM Tris pH 8.0, 300 mM NaCl, 10 mM imidazole, 10% glycerol, 5 mM β-mercaptoethanol, and 100 mM phenylmethylsulfonyl fluoride (PMSF), and frozen at −80 °C until further use. Cells were lysed using a Microfluidizer system (Microfluidics). The clarified lysate was bound over a nickel-nitrilotriacetic acid (Ni-NTA) column for affinity purification. H_6SUMO-tagged proteins were cleaved by Ulp1-his protease (36). Proteins were then purified using size-exclusion and anion-exchange chromatography using Sephacryl 200 16/60 and MonoQ 5/50 columns. ClpX and ClpP were purified as outlined in ref. 9. Detailed purification protocols are available upon request. For all in vitro experiments, RcdA concentrations are stated in terms of monomeric equivalents unless otherwise noted.

Cloning and Molecular Biology. RcdA variants were cloned using around-the-horn, site-directed mutagenesis by amplifying the desired plasmid using pET23SUMO-RcdA as a template. To generate the *ΔrcdAXylX::Pxyl* integration strains, the pXGFPN-1 plasmid (37) was used as a template to generate a vector with the RcdA, RcdA(L82E), and RcdA(3E) coding sequences under the xylose promoter. The coding sequence of RcdA, RcdA(L82E), or RcdA(3E) was amplified with complementary overlaps to this vector, and the final construct was generated using Gibson Assembly method (38). Competent *ΔrcdA Caulobacter* cells were transformed with pXGFPN-1-RcdA, RcdA(L82E), or RcdA(3E) containing plasmids and selected on 30 μg/mL spectinomycin/streptomycin plates. To generate RcdA or RcdA L82E merodiploid strains, we performed around-the-horn mutagenesis on the wild-type RcdA pENTR gateway cloning vector (EPC 721) using the same primers used to make the original L82E mutation. We transformed this plasmid into competent wild-type cells and selected on 50 μg/mL kanamycin-containing peptone-yeast extract (PYE) plates. We confirmed insertion of the L82E coding sequence by Sanger sequencing.

In Vivo Protein Stability and Synchrony Assays. Wild-type or *Caulobacter* cells expressing different constructs from a xylose inducible promoter or from the native *rcdA* locus were grown in PYE media with appropriate antibiotic and xylose when required as outlined in the figure legends. Cells were grown to an OD$_{600}$ of ∼0.4 with addition of 0.2 to 0.002% xylose or 0.2% glucose (when noted). Protein synthesis was blocked by the addition of 30 μg/mL chloramphenicol, and aliquots were taken at the time points indicated in the figures. For synchrony experiments, an asynchronous population of cells was grown to an OD$_{600}$ of ∼0.4 in PYE. Swarmer cells were harvested and isolated using Percoll density gradient centrifugation and then released into fresh PYE media containing 0.002% xylose (when needed) for progression through the cell cycle.

Microscopy. Phase contrast microscopy was performed on glass slides layered with a 1% agarose pad. A Zeiss Scope A.1 microscope equipped with 100× (1 × 25 oil ∞/0.17) objective and 60 N-C 1″ 100× camera was used. Images were analyzed with BacStalk (Drescher Lab, Max Planck Institute) software. Stalk distributions were compared using a one-tailed unpaired *t* test with $\alpha = 0.05$ (GraphPad Prism).

Motility Assays. Motility assays were performed as described previously (36). Briefly, 0.3% agar plates containing varying concentrations of xylose and glucose were inoculated with three independent colonies of each strain for 3 d at 30 °C. Colony sizes were determined using ImageJ (NIH). Quantifications were completed using ImageJ and plotted in GraphPad Prism.

In Vivo Growth Competition Assay. Overnight cultures of a strain constitutively expressing the fluorescent reporter Venus (CPC798) were mixed with wild type, P_{rcdA}::RcdA, and P_{rcdA}::RcdA L82E at a 1:1 ratio. Mixed strains were then diluted 1:15,000 into fresh media and allowed to outgrow for 24 h. The initial 1:1 mixture of cells was verified by phase contrast and fluorescence microscopy. Quantification of >100 cells was performed for three biological replicates. All final ratios were normalized to their starting ratios prior to dilution. Statistical analysis was performed using an unpaired *t* test in GraphPad Prism.

Western Blot Analysis. Aliquots withdrawn at indicated time points were spun down, resuspended in 2× sodium dodecyl sulphate sample buffer, boiled at 95 °C for 10 min, and then centrifuged. After centrifugation, 10 μL clarified supernatant was loaded onto sodium dodecyl sulphate-polyacrylamide gel electrophoresis gels. Proteins were then transferred onto a nitrocellulose membrane at 20 V for 1 h and probed for monoclonal rabbit anti-RcdA (1:5,000), monoclonal rabbit anti-ClpP (1:5,000), polyclonal rabbit anti-SpbR (1:5,000), rabbit anti-FtsZ (1:5,000), or rabbit anti-CtrA (1:5,000). Following overnight primary probing at 4 °C, the membranes were washed three times with tris buffered saline with Tween (TBST). Proteins were then visualized using IRdye-labeled goat anti-rabbit antibody (LI-COR Biosciences) at 1:10,000 dilution and an Odyssey Scanning system (LI-COR).

Fluorescence Polarization and Maleimide Labeling. Purified RcdA or RcdA mutants were labeled with Fluorescin-5-Maleimide (Thermo Scientific). Purified protein at ∼8 to 10 mg/mL was buffer exchanged into labeling buffer (50 mM Tris pH 7.0, 150 mM NaCL, and 2 mM tris(2-carboxyethyl)phosphine [TCEP]). Fluorescin-5-Maleimide was dissolved in DSMO and added to protein at a 20-fold molar excess to cysteine. Labeling reactions were completed at 4 °C overnight. Free dye was removed using a PD-MidiTrap column (GE Healthcare) and Amicon Ultra-15 Centrifugal Filter Units in a buffer containing 20 mM Hepes pH 8.5, 100 mM KCl (potassium chloride) 10 mM $MgCl_2$ (magnesium chloride), and 0.05% Tween. Confirmation of protein labeling was verified using a Typhoon imaging system (GE Healthcare). The labeled protein was aliquoted and flash frozen at −80 °C.

Fluorescence polarization binding experiments were performed with 100 nM labeled RcdA or RcdA L82E and varying concentrations of cargo. The binding reaction was incubated at 25 °C for 1 h to reach equilibrium. Polarization measurements were read from 40 uL of these mixtures using opaque black 384-well plates and a SpectraMax M5 plate reader (Molecular Devices), with excitation and emission wavelengths set at 460 and 540, respectively. Equilibrium binding constants were calculated by fitting the polarization data using GraphPad Prism to a one site, total, and nonspecific binding equation, $P = Pmax \times [X]/([X] + K_D) + NS \times [X] + Background$, where Pmax is the maximum specific binding value, *P* is the polarization value, NS is the slope of linear nonspecific binding constrained to be greater than 0, and the background is the polarization value when [X] is 0. Error bars are calculated from the SD between replicates of experiments. All RcdA concentrations are in terms of monomeric equivalents unless otherwise noted.

Chemical Cross-Linking. For cross-linking experiments, 100 μM RcdA or L82E was incubated with increasing concentrations of glutaraldehyde as annotated. Cross-linking was performed in 20 mM Hepes buffer, pH 7.5, with 100 mM KCl and quenched after 2 h of incubation at room temperature with 1 M Tris pH 8. The resulting mixture was then desalted into the same Hepes buffer used for fluorescence polarization experiments.

Isothermal Titration Calorimetry. Isothermal Titration Calorimetry (ITC) experiments were completed using a Malvern-autoiTC200 automated system (Malvern). Measurements were taken at 25 °C. The reference cell was filled with 20 mM Hepes pH 8.5, 100 mM KCL, and 10% glycerol. This buffer was used for all ITC experiments and for dialysis of each protein into the same buffer prior to the experiment. The sample cell was loaded with 400 μL of 40 μM SpbR, and the stirring syringe was loaded with 120 μL of 400 μM RcdA. A total of 19 injections of RcdA into SpbR were used to build the binding isotherm. Data analysis was performed with MicroCal (ORIGIN) and fitted to a single set of identical sites equation $K_D = (\Theta)/((1-\Theta) \times [X])$, where Θ is the fraction of sites occupied by ligand X, and [X] is the concentration of ligand X. For dimer dissociation, the sample cell was loaded with 400 μL of the buffer described above, and the stirring syringe was loaded with 120 μL of 400 μM RcdA. Dissociation data were fit to the dimer dissociation model in ORIGIN ($P^2 > 2P$)

Size-Exclusion Chromatography with Multiangle Light Scattering. Each protein complex was allowed to bind at room temperature for 45 min. The complexes were then injected onto a TSKgel G3000 SEC column equilibrated in 20 mM Hepes buffer, pH 7.0, with 100 mM KCL and 10% glycerol (Tosoh Biosciences) at room temperature. The SEC column was coupled to an 18-angle light scattering detector (DAWN HELEOS-II) and a refractive index detector (Optilab T-rEX) (Wyatt Technology). Data were collected every second, and the flow rate was set to 0.5 mL/min. Data analysis was carried out using the program ASTRA (Wyatt Technology). Monomeric bovine serum albumin (Sigma) was used for calibration of the light scattering detectors and general data quality control. Measurements were taken at 25 °C. The light scattering data were collected across a window containing the entire chromatographic peak for a full distribution of molecular weights shown underneath each chromatogram. The monomeric equivalent concentrations used in the SEC-MALS experiments are as follows, unless otherwise noted in the figure legends: 25 μM RcdA, 25 μM RcdA L82E, 25 μM RcdA 3E, 50 μM PopA, 50 μM SpbR, and 15 μM His-TacA. We used 50 μM RcdA and SpbR for Figs. 1 and 3. The concentrations we used in our coelutions studies were the same concentrations used in our SEC-MALS studies.

Microscale Thermophoresis. The microscale thermophoresis (MST) experiments were performed using a Monolith NT.115 instrument (NanoTemper). Fluorescin-5-Maleimide–labeled RcdA was incubated with increasing concentrations of unlabeled RcdA in the same buffer used in the polarization experiments. The measurements were performed at 20% MST power with 40% light emitting diode power and with 3 s laser on time and 25 s off time. The K_D values were calculated using MO.Affinity Analysis software (NanoTemper) and fit to the nonlinear equation, Fnorm = [unbound + (bound-unbound)/2 × (FluoConc + c + K_D − Sqrt((FluoConc + c + K_D)^2 − 4 × FluoConc × c)], where unbound and bound are the thermophoresis values of the unbound and bound states, FluoConc is the fixed concentration of the fluorophore, Fnorm is the normalized fluorescence, and c is the concentration of the unlabeled protein.

HDX-MS. Hydrogen–deuterium exchange was measured on a Synapt G2Si high-definition mass spectrometer (Waters). Deuterium exchange and quenching steps were performed using an automated HDX robotics platform (Waters). Samples were diluted 1:16 in D_2O-containing buffer containing 0.1 mM K_2HPO_4 to final concentrations, as specified in the figure legends. Deuterium exchange was allowed to take place for 0, 1, 10, and 60 min at 25 °C, with staggered starts for each dilution reaction. After all reactions were completed, aliquots were removed and diluted 1:2 into cold quench buffer at 4 °C (water with 4 M Guanidine Hydrochloride at pH 2.5) and subsequently run over an immobilized Waters ENZYMATE immobilized pepsin column (inner diameter: 2.1 × 30 mm) at a flow rate of 0.15 mL/min at high pressure (∼11,000 psi) for peptide digestion. Prior to HDX analysis, the quality of each sample was assessed using sodium dodecyl sulphate-polyacrylamide gel electrophoresis and size-exclusion chromatography.

Three independently prepared experimental replicates and labeling reactions were performed for each condition and averaged in the peptide uptake plots. Blank runs were run in between each analysis to avoid peptide carry over. Continuous lock-mass correction was performed using leu-enkephalin compound. Time points and analysis were randomized to ensure no biasing of results and to ensure variation. Peptides were ionized and separated by electrospray ionization for analysis at a mass resolution of 50 to 2,000 *m/z* range. Identification of peptides and analysis of the uptake plots and charge states for each peptide were completed in Protein Lynx Global Server and the software DynamX (Waters). Differential uptake heatmaps and uptake plots were plotted and created in Adobe Illustrator and in GraphPad Prism. Protections of greater than 15% are shown on the surface renditions of the RcdA structure (Protein Data Bank 3CTW) using PyMol (Schrodinger Software).

In Vitro Degradation Assays. Degradation of proteins was monitored using sodium dodecyl sulphate-polyacrylamide gel electrophoresis gels as described previously (21). The concentrations of different proteins used in degradation reactions are indicated in the figure legends. Degradation of GFP-CtrARD+15 was monitored with the loss of fluorescence over time, as described previously (18). The concentrations of each protein used in the reactions were as follows unless otherwise noted: 3 μM RcdA, 3 μM RcdA(L82E), 3 μM RcdA(3E), 2 μM CpdR, 0.2 μM $ClpX_6$, 0.4 μM $ClpP_{14}$, 1 μM GFP-^{DBD}TacA, 4 μM SpbR, 4 μM TacA, 2 μM GFP-CtrARD+15, and 5 mM ATP. For GFP-CtrARD+15 experiments in Fig. 6*C*, we used 1 uM GFP-CtrARD+15, 500 nM PopA, 1 μM CdG, 300 nM RcdA or L82E, 0.1 μM ClpX, and 0.2μM ClpP. GFP-CtrARD+15 and GFP-^{DBD}TacA curves were fit to a modified hyperbolic equation, with the form of $Y = ((V_{max} \times [RcdA])/(K_{act} + [RcdA])) + A$, where A is a baseline constant, or to the Michaelis–Menten equation using GraphPad Prism.

Sedimentation Velocity Analytical Ultracentrifugation. Sedimentation velocity experiments were completed using a Beckman ProteomeLab XL-1 Analytical Ultracentrifuge (Beckman). Samples were diluted into 20 mM Hepes pH 8.5, 100 mM KCl, and 10% glycerol at the concentrations indicated in the figure legends. The samples were spun at 55,000 × *g* overnight at 25 °C. The ρ and v values used for data fitting were determined using SEDNTERP and the amino acid sequence for each protein. The sedimentation velocity data were directly fit to the c(s) distribution method using the program SEDFIT and using the first 100 velocity scans for each condition. The resulting distributions from each experiment were then plotted in GraphPad Prism. The final concentrations used were the same concentrations used in the SEC-MALS experiments.

Data Availability. All study data are included in the article and/or *SI Appendix*.

ACKNOWLEDGMENTS. We thank the members of the P.C., Strieter, Stratton, and Serio laboratories for helpful comments and discussions. We thank A. Kosowicz, W. Chowdhury, and M. Sutherland for their prior work on the RcdA variants and generating plasmids. The anti-SpbR, anti-RcdA, and anti-FtsZ antibodies were graciously provided by G. Bowman, L. Shapiro, and E. Goley. This project was supported by funds from the NIH (NIH Grant R35GM130320 to P.C.); N.J.K. was supported in part through the Biotechnology Training Program (NIH Grant T32GM108556). SEC-MALS, ITC, analytical ultracentrifugation, and MST data were obtained at the University of Massachusetts Amherst Biophysical Characterization Facility. HDX-MS data were obtained at the University of Massachusetts Amherst Mass Spectrometry Facility, RRID:SCR_019063. Special thanks to Lizz Bartlett (biophysical characterization) and Steve Eyles (mass spectrometry) for their experimental and analytical assistance.

1. S. A. Mahmoud, P. Chien, Regulated proteolysis in bacteria. *Annu. Rev. Biochem.* **87**, 677–696 (2018).
2. K. N. Truscott, A. Bezawork-Geleta, D. A. Dougan, Unfolded protein responses in bacteria and mitochondria: A central role for the ClpXP machine. *IUBMB Life* **63**, 955–963 (2011).
3. A. O. Olivares, T. A. Baker, R. T. Sauer, Mechanical protein unfolding and degradation. *Annu. Rev. Physiol.* **80**, 413–429 (2018).
4. R. T. Sauer, T. A. Baker, AAA+ proteases: ATP-fueled machines of protein destruction. *Annu. Rev. Biochem.* **80**, 587–612 (2011).
5. N. J. Kuhlmann, P. Chien, Selective adaptor dependent protein degradation in bacteria. *Curr. Opin. Microbiol.* **36**, 118–127 (2017).
6. I. Levchenko, M. Seidel, R. T. Sauer, T. A. Baker, A specificity-enhancing factor for the ClpXP degradation machine. *Science* **289**, 2354–2356 (2000).
7. P. Chien, R. A. Grant, R. T. Sauer, T. A. Baker, Structure and substrate specificity of an SspB ortholog: Design implications for AAA+ adaptors. *Structure* **15**, 1296–1305 (2007).
8. J. M. Flynn, I. Levchenko, R. T. Sauer, T. A. Baker, Modulating substrate choice: The SspB adaptor delivers a regulator of the extracytoplasmic-stress response to the AAA+ protease ClpXP for degradation. *Genes Dev.* **18**, 2292–2301 (2004).
9. K. K. Joshi, M. Bergé, S. K. Radhakrishnan, P. H. Viollier, P. Chien, An adaptor hierarchy regulates proteolysis during a bacterial cell cycle. *Cell* **163**, 419–431 (2015).
10. A. A. Iniesta, P. T. McGrath, A. Reisenauer, H. H. McAdams, L. Shapiro, A phosphosignaling pathway controls the localization and activity of a protease complex critical for bacterial cell cycle progression. *Proc. Natl. Acad. Sci. U.S.A.* **103**, 10935–10940 (2006).
11. J. Lau, L. Hernandez-Alicea, R. H. Vass, P. Chien, A phosphosignaling adaptor primes the AAA+ protease ClpXP to drive cell cycle-regulated proteolysis. *Mol. Cell* **59**, 104–116 (2015).
12. P. T. McGrath, A. A. Iniesta, K. R. Ryan, L. Shapiro, H. H. McAdams, A dynamically localized protease complex and a polar specificity factor control a cell cycle master regulator. *Cell* **124**, 535–547 (2006).
13. K. C. Quon, G. T. Marczynski, L. Shapiro, Cell cycle control by an essential bacterial two-component signal transduction protein. *Cell* **84**, 83–93 (1996).
14. A. Reisenauer, K. Quon, L. Shapiro, The CtrA response regulator mediates temporal control of gene expression during the Caulobacter cell cycle. *J. Bacteriol.* **181**, 2430–2439 (1999).
15. U. Jenal, T. Fuchs, An essential protease involved in bacterial cell-cycle control. *EMBO J.* **17**, 5658–5669 (1998).
16. S. Ozaki *et al.*, Activation and polar sequestration of PopA, a c-di-GMP effector protein involved in Caulobacter crescentus cell cycle control. *Mol. Microbiol.* **94**, 580–594 (2014).
17. A. Duerig *et al.*, Second messenger-mediated spatiotemporal control of protein degradation regulates bacterial cell cycle progression. *Genes Dev.* **23**, 93–104 (2009).
18. S. C. Smith *et al.*, Cell cycle-dependent adaptor complex for ClpXP-mediated proteolysis directly integrates phosphorylation and second messenger signals. *Proc. Natl. Acad. Sci. U.S.A.* **111**, 14229–14234 (2014).
19. H. Wang, G. R. Bowman, SpbR overproduction reveals the importance of proteolytic degradation for cell pole development and chromosome segregation in Caulobacter crescentus. *Mol. Microbiol.* **111**, 1700–1714 (2019).
20. E. G. Biondi *et al.*, A phosphorelay system controls stalk biogenesis during cell cycle progression in Caulobacter crescentus. *Mol. Microbiol.* **59**, 386–401 (2006).
21. N. H. Bhat, R. H. Vass, P. R. Stoddard, D. K. Shin, P. Chien, Identification of ClpP substrates in Caulobacter crescentus reveals a role for regulated proteolysis in bacterial development. *Mol. Microbiol.* **88**, 1083–1092 (2013).
22. J. A. Taylor, J. D. Wilbur, S. C. Smith, K. R. Ryan, Mutations that alter RcdA surface residues decouple protein localization and CtrA proteolysis in Caulobacter crescentus. *J. Mol. Biol.* **394**, 46–60 (2009).
23. K. K. Joshi, M. Sutherland, P. Chien, Cargo engagement protects protease adaptors from degradation in a substrate-specific manner. *J. Biol. Chem.* **292**, 10973–10982 (2017).
24. L. Konermann, J. Pan, Y.-H. Liu, Hydrogen exchange mass spectrometry for studying protein structure and dynamics. *Chem. Soc. Rev.* **40**, 1224–1234 (2011).
25. M. J. Chalmers, S. A. Busby, B. D. Pascal, G. M. West, P. R. Griffin, Differential hydrogen/deuterium exchange mass spectrometry analysis of protein-ligand interactions. *Expert Rev. Proteomics* **8**, 43–59 (2011).
26. J. R. Aretakis, A. Gega, J. M. Schrader, Absolute measurements of mRNA translation in Caulobacter crescentus reveal important fitness costs of vitamin B_{12} scavenging. *mSystems* **4**, e00170-19 (2019).
27. M. Brilli *et al.*, The diversity and evolution of cell cycle regulation in alpha-proteobacteria: A comparative genomic analysis. *BMC Syst. Biol.* **4**, 52 (2010).
28. F. Pini *et al.*, Cell cycle control by the master regulator CtrA in Sinorhizobium meliloti. *PLoS Genet.* **11**, e1005232 (2015).
29. H. W. Kim *et al.*, Skp1 dimerization conceals its F-box protein binding site. *Biochemistry* **59**, 1527–1536 (2020).
30. B. L. Brown *et al.*, N domain of the Lon AAA+ protease controls assembly and substrate choice. *Protein Sci.* **28**, 1239–1251 (2019).
31. S. Gottesman, E. Roche, Y. Zhou, R. T. Sauer, The ClpXP and ClpAP proteases degrade proteins with carboxy-terminal peptide tails added by the SsrA-tagging system. *Genes Dev.* **12**, 1338–1347 (1998).
32. K. E. McGinness, D. N. Bolon, M. Kaganovich, T. A. Baker, R. T. Sauer, Altered tethering of the SspB adaptor to the ClpXP protease causes changes in substrate delivery. *J. Biol. Chem.* **282**, 11465–11473 (2007).
33. D. N. Bolon, D. A. Wah, G. L. Hersch, T. A. Baker, R. T. Sauer, Bivalent tethering of SspB to ClpXP is required for efficient substrate delivery: A protein-design study. *Mol. Cell* **13**, 443–449 (2004).
34. I. Levchenko, R. A. Grant, D. A. Wah, R. T. Sauer, T. A. Baker, Structure of a delivery protein for an AAA+ protease in complex with a peptide degradation tag. *Mol. Cell* **12**, 365–372 (2003).
35. K. C. Keiler, Mechanisms of ribosome rescue in bacteria. *Nat. Rev. Microbiol.* **13**, 285–297 (2015).
36. K. L. Rood, N. E. Clark, P. R. Stoddard, S. C. Garman, P. Chien, Adaptor-dependent degradation of a cell-cycle regulator uses a unique substrate architecture. *Structure* **20**, 1223–1232 (2012).
37. M. Thanbichler, A. A. Iniesta, L. Shapiro, A comprehensive set of plasmids for vanillate- and xylose-inducible gene expression in Caulobacter crescentus. *Nucleic Acids Res.* **35**, e137 (2007).
38. D. G. Gibson *et al.*, Enzymatic assembly of DNA molecules up to several hundred kilobases. *Nat. Methods* **6**, 343–345 (2009).